



Machine learning for sinkhole risk mapping in Guidonia-Bagni di Tivoli plain (Rome), Italy

Silvia Bianchini, Pierluigi Confuorto, Emanuele Intrieri, Paolo Sbarra, Diego Di Martire, Domenico Calcaterra & Riccardo Fanti

To cite this article: Silvia Bianchini, Pierluigi Confuorto, Emanuele Intrieri, Paolo Sbarra, Diego Di Martire, Domenico Calcaterra & Riccardo Fanti (2022): Machine learning for sinkhole risk mapping in Guidonia-Bagni di Tivoli plain (Rome), Italy, Geocarto International, DOI: [10.1080/10106049.2022.2113455](https://doi.org/10.1080/10106049.2022.2113455)

To link to this article: <https://doi.org/10.1080/10106049.2022.2113455>



© 2022 The Author(s). Published by Informa UK Limited, trading as Taylor & Francis Group



Published online: 08 Sep 2022.



Submit your article to this journal [↗](#)



Article views: 394



View related articles [↗](#)



View Crossmark data [↗](#)

Machine learning for sinkhole risk mapping in Guidonia-Bagni di Tivoli plain (Rome), Italy

Silvia Bianchini^a , Pierluigi Confuorto^a , Emanuele Intrieri^a, Paolo Sbarra^a,
Diego Di Martire^b , Domenico Calcaterra^b  and Riccardo Fanti^a

^aEarth Sciences Department, University of Florence, Florence, Italy; ^bEarth, Environment and Resource Sciences Department, University of Naples Federico II, Naples, Italy

ABSTRACT

This work presents a sinkhole susceptibility and risk assessment mapping in Guidonia-Bagni di Tivoli plain (Italy), a travertine sinkhole-prone area where sudden occurrences of sinkholes have happened in past and recent times. We collected a point-like sinkhole inventory and we considered a series of different sinkhole-controlling and precursory factors over the study area, related to its geo-litho-hydrological setting and to its terrain deformational scenario, i.e. ground motion rates derived from InSAR COSMO-SkyMed imagery. A sinkhole susceptibility map was produced through a machine learning model, namely Maximum Entropy algorithm (*MaxEnt*). Results highlight that the most determining factors for sinkhole formation are the lithology, the travertine thickness, groundwater and the land use. The sinkhole susceptibility map was then combined with data on vulnerability and elements-at-risk economic exposure in order to provide a sinkhole risk map of the area. The outcomes show that areas at higher risk covers about 2% of the total study area and primarily relies on the zoning of the main urban fabric. In particular, it is worth to highlight that 5% of the whole road-network pavement and 27% of all the residential buildings fall into High and Very High risk classes. Overall, results of this work demonstrate capabilities of machine learning models to assess sinkhole susceptibility for predicting potential sinkhole areas, and provide a sinkhole risk map, along with information on urban environment, as a useful tool for urban planning and geohazard risk management.

ARTICLE HISTORY

Received 17 May 2022
Accepted 10 August 2022

KEYWORDS

Sinkhole; susceptibility risk; machine learning; maximum entropy algorithm; Guidonia-Tivoli plain

1. Introduction

Sinkholes are depressions in the ground caused by some forms of lowering or sudden collapse of the surface layer, induced by the erosion of subsurface rocks (Billi et al. 2016).

Sinkholes are usually classified with respect to the ground failure mechanisms and the involved material. In accordance with their formational processes, solution sinkholes,

CONTACT Silvia Bianchini  silvia.bianchini@unifi.it

© 2022 The Author(s). Published by Informa UK Limited, trading as Taylor & Francis Group
This is an Open Access article distributed under the terms of the Creative Commons Attribution-NonCommercial-NoDerivatives License (<http://creativecommons.org/licenses/by-nc-nd/4.0/>), which permits non-commercial re-use, distribution, and reproduction in any medium, provided the original work is properly cited, and is not altered, transformed, or built upon in any way.

collapse sinkholes, deep piping and suffosion sinkholes can be distinguished (Waltham et al. 2005).

Sinkholes result from different concurrent or sequential processes such as hydrogeological processes, e.g. subsurface dissolution by groundwater flow, and mechanical processes, e.g. downward gravitational movement of the overlying material. Thus, several mechanisms can trigger sinkholes: whilst the process of gradual chemical dissolution of soluble rocks (e.g. carbonate or evaporite) can cause a sinkhole (Watson et al. 2019), many factors can favour sinkholes to develop (Yilmaz 2007). The hydrographical setting is considered as a conditioning factor for sinkhole occurrence in many scientific works that analyze the drainage system and the hydrological conditions for channel, voids and collapse formation in karst (e.g. Galve et al. 2009; Ciotoli et al. 2016; Ozdemir 2016; Intrieri et al. 2018; Kaufmann and Romanov 2019; Al-Halbouni et al. 2021). Groundwater circulation and the hydrogeological setting are relevant facets for sinkholes occurrence, as the presence of water in the subsoil can generate hydrofracturing and karst processes, fostering cavities and ground collapses (Gutiérrez et al. 2014). Sinkhole formation can be also triggered by geothermal and seismic processes (Del Prete et al. 2010; Billi et al. 2016, 200; La Rosa et al. 2018) or can be induced by tectonic elements, i.e. faults that represent preferred pathways for the rising of deep fluids (Santo et al. 2012). Moreover, extensive literature shows that many anthropogenic activities, such as groundwater withdrawal, building works, irrigation and dewatering for mining activities greatly increase the occurrence of new sinkholes (Parise and Vennari 2013; Taheri et al. 2015).

Sinkhole occurrence in urbanized areas is a major hazard that can cause relevant economic and social damage in terms of losses in human lives, and severe injuries to structures and infrastructures (Galve et al. 2011; Ammirati et al. 2020). Sinkholes are an increasingly serious urban-planning problem worldwide: some examples to be mentioned are in the USA in America (e.g. Gao and Alexander 2008; Kim et al. 2020), Italy and Spain in Europe (e.g. Galve et al. 2009; Del Prete et al. 2010; Rispoli et al. 2020; Esposito et al. 2021), Iran, Turkey and China in Asia (e.g. Kemmerly 1993; Jiang et al. 2005; Nof et al. 2013; Orhan et al. 2020;), South Africa in Africa (Theron et al. 2017). Furthermore, when sinkholes occur on agricultural lands, they also can cause reduction of arable land, damage to factories and rural buildings and thus can determine relevant economic impact for cultivation activity (Ozdemir 2016; Dursun 2022).

In order to assess sinkholes hazard and risk, it is essential to map the spatial likelihood of these collapsing events with the aim of preventing damages and managing land-use activities in sinkhole-prone areas. Nevertheless, this is a complex and difficult task since the formation of sinkholes is often sudden and unpredictable. The first step towards an accurate sinkhole risk evaluation is the production of a susceptibility zonation map. The susceptibility of an area to a certain phenomenon is defined as the spatial predisposition of that area to the phenomenon occurrence on the basis of local geoenvironmental factors (Guzzetti et al. 2006). Such susceptibility zonation relies on the principle of *actualism*, according to which future phenomena will happen under the same conditions that caused the past ones (Bianchini et al. 2016). A sinkhole susceptibility zoning map based on predictive analyses through a probabilistic approach is fostered to study the interactions between existing sinkholes, environmental conditioning factors and future potential occurrences, for urban planning and geohazard management purposes.

A sinkhole susceptibility map aims to detect areas potentially affected by sinkhole occurrence, starting from existing archives or inventories of sinkholes (Guarino et al. 2017; Tufano et al. 2022) in order to know where they happened in the past, and from the identification of the main controlling factors.

In scientific literature, sinkhole susceptibility mapping has been performed in the last decade by using GIS (Geographic Information System) technology and various methods, i.e. heuristic approaches based on geo-morphologic expertise and geophysics (Forth et al. 1999; Kaufmann and Quinif 2002; Koutepov et al. 2008; Pazzi et al. 2018; Watson et al. 2019), statistical approaches such as logistic regression (Ozdemir 2016) analytic hierarchy process (Jiang et al. 2005; Taheri et al. 2015), frequency ratio (Yilmaz 2007; Galve et al. 2011), artificial neural networks (Kim et al. 2020). These methods provide sinkhole susceptibility maps as spatially continuous and simply accessible tools for the management of sinkhole-related hazard (Galve et al. 2009). In some cases, Ground-Based Interferometric Synthetic Aperture Radar systems (GB-InSAR) and satellite InSAR data have been also included in susceptibility and hazard approaches as measurements of ground motion rates for detecting land subsidence and sinkhole precursory deformation (e.g. Nof et al. 2013; Intrieri et al. 2015; Theron et al. 2017; Esposito et al. 2021).

In this work, we explore a new approach for sinkhole susceptibility mapping by means of a machine learning algorithm named *MaxEnt* (Maximum Entropy) based on maximum entropy modelling. This algorithm has been originally conceived for biodiversity and ecology modelling, but it can be successfully applied for analyzing other complex environmental problems (Çoban et al. 2020; Phillips et al. 2021) and hazards, such as landslides (Felicísimo et al. 2013; Di Napoli et al. 2020; Raso et al. 2020). To our knowledge, Maximum Entropy machine learning method has not been exploited for modelling sinkhole zonation maps.

Beyond susceptibility, risk assessment requires computing the vulnerability and the exposure of the elements at risk over the study area. Sinkhole risk assessment models have been developed in scientific literature to evaluate the expected degree of damage and loss that are inherent to the sinkhole hazard for a given area, by taking into account the zoning and characterization of sites in terms of the hazard within a framework of well-defined predisposing factors, the types of land development (Buttrick and Van Schalkwyk 1998) and the economic exposure and costs of indirect financial damage (Giampaolo et al. 2016; Toulkeridis et al. 2016).

Since such a risk evaluation requires the parameterization and the combination of a high number of detailed geomorphological and socio-economic factors, it is usually performed qualitatively and at a local scale by the research community, while only a few works deals with large scale risk assessment, e.g. Jiang et al. (2005), who present a national-scale sinkhole risk assessment in China or Gao and Alexander (2008), who provide a sinkhole zoning assessment over the whole Minnesota, USA.

The vulnerability accounts for the likelihood to damage of the assets exposed to the geohazard and can be defined as the degree of loss experienced by the elements at risk for a given intensity (Glade and Crozier 2005). The exposure represents the stock of property and infrastructure exposed to the geohazard, and it includes location, types, attributes, and socio-economic value of the assets.

The sinkhole vulnerability corresponds to the expected degree of damage due to sinkhole impact on a human element, ranging from 0 (no damage) to 1 (total disruption). It depends on both the intensity of the phenomenon, and on the resistance of different elements at risk (EAR) on the territory. A few sinkhole vulnerability classification systems have been proposed in scientific literature. Relationships can be constructed by establishing a correspondence between vulnerability and the intensity of the hazardous process, e.g. sinkhole type and size. For instance, Buttrick and Van Schalkwyk (1998) studied sinkholes in South Africa and considered the sinkhole diameter and depth as reference data for the intensity of the phenomenon. Another approach consists in classifying the EAR based on

the main land use and structures (urban, industrial, agricultural infrastructures) and their importance in the local economy (Papathoma-Köhle et al. 2007). For instance, Bianchi Fasani et al. (2013) subdivided the elements at risk into a simple system of four classes, accounting for scattered or continuous urban fabric, construction and foundation type, and hierarchical order of roads. Otherwise, vulnerability can be assessed on the basis of data about economic and human losses caused by sinkholes in the past or by numerical modeling (Gutiérrez et al. 2014). In this work the vulnerability to sinkholes over the study area has been derived by solely considering the type of the different Elements At Risk (EAR).

Results of sinkhole susceptibility mapping area were integrated with data on the vulnerability of the elements at risk, whose values were calculated according to the typology of the exposed land use and structures, and to the economic exposure derived from cadastral inventories, market and income values and bibliographic references, in order to produce a sinkhole risk zonation map.

The study area of this work is the Guidonia-Bagni di Tivoli plain (central Italy), which is an area historically threatened by sinkholes occurrence (Billi et al. 2016). The geohydrogeological and structural features of the Guidonia-Bagni di Tivoli plain make the area prone to various karst and hyperkarst processes (Nisio et al. 2007; Centamore et al. 2009; Floris et al. 2014; Ozdemir 2016). Buried *collapse* and *deep piping sinkholes* filled with soil and regolith are common in the travertine substratum of this geothermal-seismic area. Moreover, travertine quarry activities in the area and the load of buildings due to urbanization accelerate the development of subsurface cavities in the travertine plateau (De Ritis et al. 2020).

Many buildings have been recently damaged due to ground subsidence and sinkholes (Brunetti et al. 2013; Rinalduzzi et al. 2017). The available sinkhole inventory includes poorly quantitative geometrical data on sinkholes (e.g. lacking information about depth and size of mapped collapses) and it comprises different information records of modern sinkholes occurrences as well as surveys of locations of ancient sinkholes from bibliographic references.

Overall, our research aims at illustrating the development of sinkhole risk mapping in the study area by quantitatively assessing the sinkhole controlling factors and their spatial distribution throughout machine learning model, and by evaluating in GIS environment the associated risk in terms of expected value of loss, as a useful tool for urban planning and geohazard risk management.

The assumptions and methodologies presented in this work could be reproduced in other test areas where few information is available on sinkhole occurrences due to a large scale of analysis or to scant or incomplete sinkhole inventory (e.g. poor availability of quantitative geometric data on sinkhole events), in order to check the used modelling performance in different environmental and geological settings.

2. Study area

The selected study area of the work extends over an area of about 38 km² within the Guidonia-Bagni di Tivoli plain, which is located in a Plio-Pleistocene, geothermally- and seismically-active basin, near Rome, in Lazio region (central Italy), also known by the name of Acque Albule basin (Figure 1a). This area is characterized by a thick deposit of late Pleistocene thermogenic travertine, which has been historically quarried, and it is threatened by land subsidence and sinkholes, due to collapse for water percolation in karst travertine structures and to dissolution and deep piping for the upwelling of mineralized high-pressure water (Billi et al. 2016; Ciotoli et al. 2016).

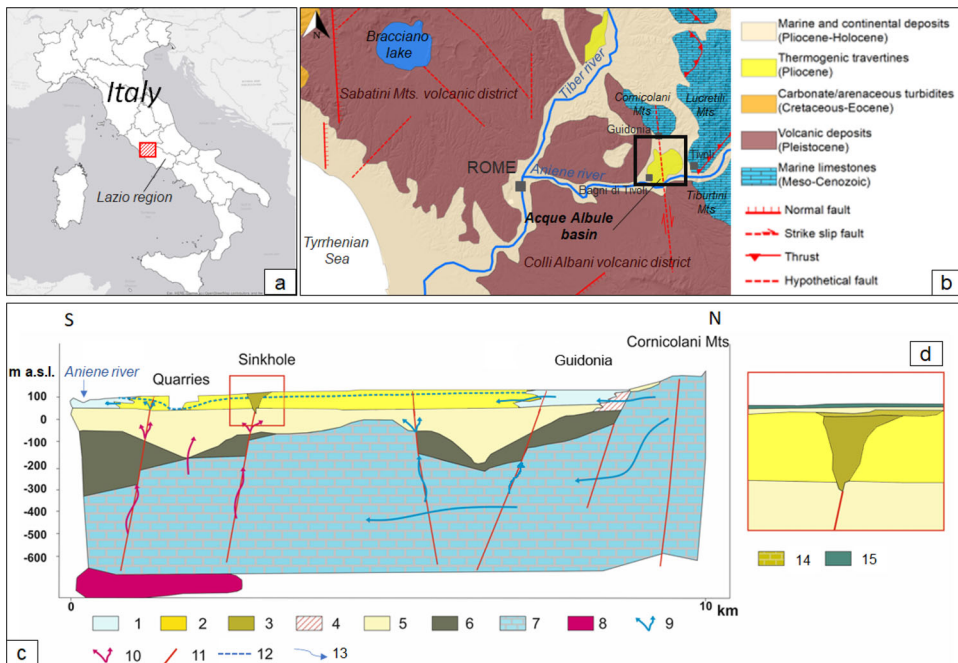


Figure 1. (a) Geographical location of the study area; (b) Geological framework map the Guidonia-Bagni di Tivoli plain; (c) Conceptual model of the hydrogeological and structural asset of the Acque Albule basin, depicted as hypothetical 2D cross-section with general N-S direction. The red-frame refers to a potential buried *deep piping sinkhole* example, which is shown more in the detail in the right box (d). Legend: (1) Holocene deposits; (2) Lithoid travertine; (3) soil fill; (4) Colluvial deposits; (5) Pleistocene clayey deposits; (6) Pliocene deposits; (7) Meso-Cenozoic carbonate deposits; (8) Thermal source; (9) Discharge and leakage of confined aquifer; (10) upwelling and leakage of thermal water; (11) Tectonic discontinuities; (12) water level of shallow aquifer; (13) main recharge and water flow direction; (14) Soil; (15) Poorly-cohesive travertine. The Layers 14 and 15 of box (d) are not drawn in box (c) due to the scale of the image (mod. from La Vigna (2009) and from De Ritis et al. (2020).

2.1. Geological and geomorphological setting

The study area is located in the Acque Albule hydrothermal basin, which is a N-S elongated sedimentary depression originated during the post-orogenic extensional tectonic phase of central Apennines. The basin is bordered southwards and westwards by the Aniense River alluvial plain (Figure 1b). From a tectonic point of view, the Acque Albule basin is considered a pull-apart basin located along the deeper branch of a N-S strike-slip right-lateral fault ('Sabina fault') that crosses the Cornicolani mountains, cuts the Aniense valley orthogonally and ends in the northern part of the Colli Albani (Gasparini et al. 2002; Faccenna et al. 2008).

The Acque Albule stratigraphical sequence, from bottom to top, is made of Meso-Cenozoic marine limestones, which also border the basin northwards and eastwards, covered by Plio-Pleistocene arenaceous deposits (i.e. Plio-Pleistocene lower marine clays and clayey sandstones, and upper continental sandy and conglomeratic deposits) and by Pleistocene volcanic products derived from the nearby Colli Albani and Sabatini volcanic districts. This sequence is overlapped by a large and thick travertine body of late Pleistocene age and thermogenic origin related to the latest magmatic manifestations of the volcanic complex and tectonic strike-slip activity, with an average thickness of 50 m and a maximum of 85 m along a N-S oriented strike-slip fault zone (Gasparini et al.

2002). Travertine is composed of a compact lithoid deposit, usually covered by a few meters of poorly-cohesive younger travertine and by regolith and soil with a thickness of few decimeters to a few meters. Holocene alluvial deposits of the Aniene river finally cover most of the plain (Argentieri et al. 2015; Billi et al. 2016).

2.2. Hydrogeological conceptual model

The present hydrogeological, geothermal and structural asset of the Acque Albule Basin is depicted as a hypothetical 2D cross-section in [Figure 1c](#). The hydrogeology of the basin is characterized by two main hydraulically-connected aquifers: the deep-confined one corresponds is hosted in Meso-Cenozoic thick carbonate succession, and the shallow one is composed of massive and highly porous Pleistocene travertine plateau, it is unconfined in most of the basin (somewhere locally semi-confined by low-hydraulically conductive surface sediments) and it is, at present, strongly dewatered by the water pumping needed to quarry deep travertine banks (Brunetti et al. 2013; Floris et al. 2014; Bozzano et al. 2015). The two aquifers are separated by a non-continuous aquiclude of Pleistocene clayey and sandy low-permeability deposits.

The hydraulic regime of the area is dominated by groundwater that infiltrates through the surrounding fractured carbonate massifs, which represents a large lateral recharge area, by the presence of striking faults and by groundwater discharge into the Aniene River.

In particular, the hydraulic circuit of the Acque Albule basin involves two groundwater circulations. The first, deep circulation mostly occurs within the carbonate bedrock, recharged by Cornicolani Mts area located N and NE of the basin, and slightly recharges surface deposits and remains confined by the clayey-sandy aquiclude. At deep levels, this huge amount of groundwater that travels in the carbonate karst aquifers is partly heated and enriched by CO₂ and other gases deriving from nearby hydrothermally-active volcanic district (Billi et al. 2016). The waters mix with warmer endogenic fluids that rise along the faults that produced the basin and dissected the Meso-Cenozoic sequence (Faccenna et al. 2008). The second, shallower circulation moves mainly N-S within the travertine aquifer and the recent deposits. It is recharged directly by rainfall, laterally by few overflowing from Cornicolani Mts carbonate aquifer and mainly by the upwelling of thermal-mineralized waters from the deep circuit. This rising of deep hydrothermal waters along tectonic discontinuities causes a mixing with shallower waters and produces many hydrothermal springs. The main N-S trending fault zone acts as preferential pathways for the upward movement of such deep fluids and most springs occur along this fault, which is partly covered by the travertine body (Faccenna et al. 2008; Brunetti et al. 2013). Furthermore, it is a seismically-active fault: seismic studies in the area documented that in 2001 low-magnitude shallow earthquake hypocenters (2 km deep at the most) were aligned along this tectonic structure in the basin and defines a striking seismically-active fault zone between about 1.5 and 0.5 km of depth beneath the travertine (Gasparini et al. 2002).

Other hydrothermalism processes also occur in the quarry areas because the quarries themselves are located on sites that are characterized by thermal rising, and also because the strong dewatering for mining activities make some hydrothermal waters to draw back into the quarry area according to the strong hydraulic gradient established.

2.3. Sinkhole occurrence and inventory

The Guidonia-Bagni di Tivoli plain is an already well-known sinkhole area as it is a geothermal-seismic area characterized by intense karst processes (Billi et al. 2016).

Just after or concurrently the late Pleistocene last volcanic phase of the nearby Colli Albani, a huge subsurface thermal groundwater, enriched in endogenic chemical elements from the volcanic complex circulated through the voids of Meso-Cenozoic marine limestones and produced the thermogenic Tivoli travertine. This pressurized and aggressive geothermal fluid circulation is still active and produces the carbonate chemical dissolution and bottom-up erosion processes of jointed strata that can trigger the sinkholes (Billi et al. 2016).

The outcropping travertine near the Aniene River has been quarried since Etruscan and Roman times (1st millennium BC) and mining has been active also during Renaissance. From the early twentieth century and mainly from the 1950s, the quarry area has been enlarged northwards, and new wider and deeper quarries have been open between Villalba and Villanova (Floris et al. 2014).

The current extraction process is facilitated by an extensive system of sumps and pump stations for dewatering the travertine aquifer and permitting mining operations at the pit floor. Such groundwater abstraction activities contribute to subsidence and thus to potential sinkhole occurrence (Brunetti et al. 2013). Furthermore, seismic shaking due to seismically-active shallow faults could have played a concurrent role in producing sudden ground collapses (Billi et al. 2016).

Sinkholes and similar surface karst phenomena as well as subsidence have been well documented in the Acque Albule Basin since historical times (Nisio et al. 2007). The area is characterized by different sinkhole typologies, mainly *cave and cover collapse sinkholes* and *deep piping sinkholes* (Waltham et al. 2005; Nisio et al. 2007; Caramanna et al. 2008). The *cave collapse sinkhole* develops in the outcropping lithoid travertines through the brittle deformation of bedrock karst material, while the *cover collapse sinkhole* refers to the quick sinking of unconsolidated cover deposits. The process is due to the percolation of water through the shallower layers that tends to widen the fractures and voids within the travertine and evolves with the subsequent collapses of the cave roof. The *deep piping sinkholes* occur in the travertine and are caused by the rising of pressurized and mineralized waters, which lead to the formation of a conduit or funnel, even at great depth (Figure 1d). In this type of sinkhole a reversed hypogeum erosion and propagation process develops from the bottom upwards and it is facilitated by the presence of faults that can represent preferential pathways for the ascension of carbonate-rich thermal waters and gases (Ciotoli et al. 2016).

Many sinkholes in the Guidonia Bagni di Tivoli are buried sinkholes since they are totally filled by unconsolidated deposits and regolith that have been compacted under the load of construction, and thus are hidden and apparently relict. Nevertheless, in both cases of *collapse sinkholes* or *deep piping sinkholes*, suffosion and other downward washing processes may lead to the sinkhole rejuvenation with reactivation of buried sinkholes and formation of new surface depressions. Hydrothermal fluid circulation or seismic shaking could also favor this sinkhole rejuvenation (Billi et al. 2016).

Some filled sinkholes and other karstic cavities are clearly visible along quarry walls (Billi et al. 2016). Many hidden sinkholes are obliterated by quarrying activities or even by overbuilding, which makes some recent buildings slowly sink (Brunetti et al. 2013; De Filippis et al. 2013; Floris et al. 2014; Bozzano et al. 2015). Villalba, Villanova and Bagni di Tivoli villages have been experiencing strong subsidence and are affected by fractures and building damage. The subsidence process started to affect buildings in the 1980s and

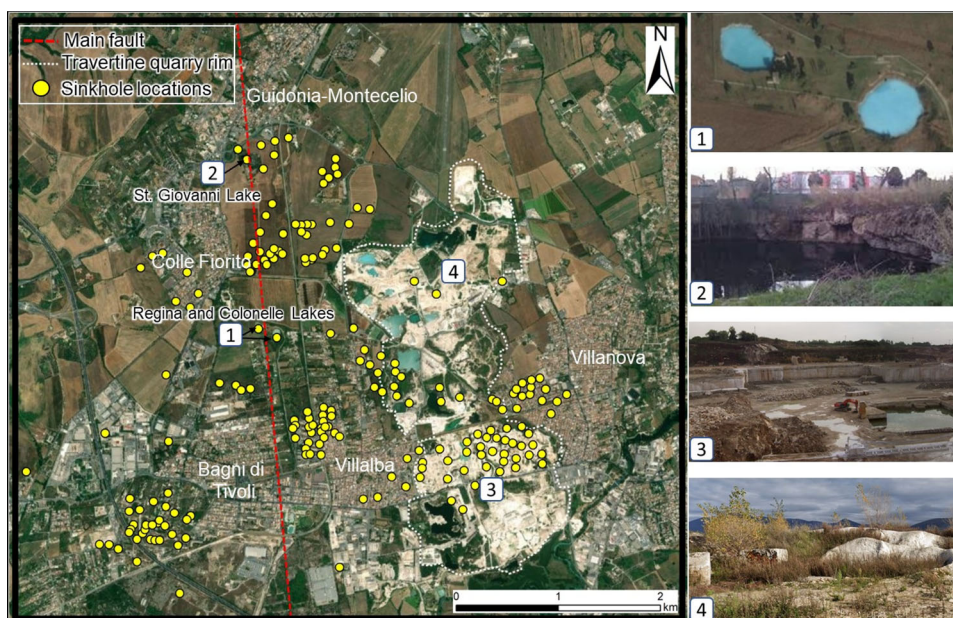


Figure 2. Point-like sinkhole inventory overlapped on orthophoto referred to June 2021. Photos on the left referred to: Regina and Colonnelle lakes (from Bing Maps© Microsoft) (1), St. Giovanni Lake (from Falcioni 2018) (2), Travertine quarrying areas (3) and deposits (from Street View © Google) (4).

increased at the beginning of the 2000s, even causing the evacuation of some houses and public buildings (Bozzano et al. 2015). Some sinkholes are presently lakes (e.g. Regina and Colonnelle lakes, actually acting as springs) or are former lakes that are dried, nowadays. Therefore, sinkholes appear irregularly distributed over the basin, potentially due to lacking information in many areas that are covered or obliterated by buildings, quarries, or vegetation.

Regarding the availability of existing sinkhole inventory in the Guidonia-Bagni di Tivoli area, previous works reported numerous sinkholes characterized by sub-circular shape and diameters ranging between a few meters and 1 km. In particular, Billi et al. (2016) provided mapping of either recently-visible sinkholes by means of aerial photographs, Digital Elevation Models (DEMs), past geomorphologic studies, field surveys and historical documents, either relict sinkholes by detailed subsurface studies through electric resistivity tomography (ERT), penetration methods (DPSH), and borehole logs.

The mapped sinkholes considered for this study account for 203 elements (points or polygons depending on the data sources) shown in Figure 2. In particular, 191 mapped geometries were derived from the work of Billi et al. (2016) and converted into points as polygon centroids, while additional 12 sinkholes were collected from the Italian National Institute for Environmental Protection and Research (ISPRA) which manages a database of point-wise sinkhole locations over the whole Italian territory (ISPRA 2022).

3. Methodology and data

We performed a GIS-based procedure for computing and mapping the sinkhole susceptibility and risk on the study area. The workflow consists of different steps (Figure 3).

Firstly, we considered eight geoenvironmental conditioning factors for sinkhole occurrence. They are seven controlling factors, i.e. lithology, land use, soft soil thickness,

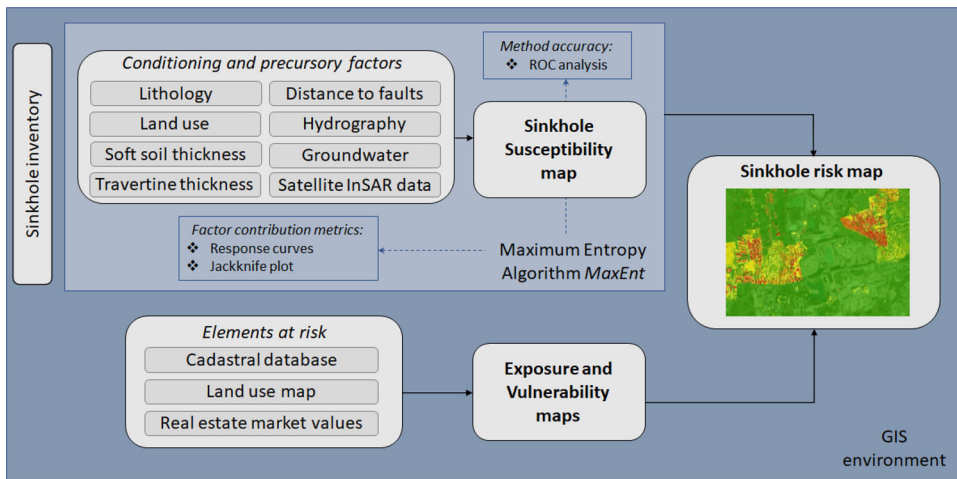


Figure 3. Methodological flowchart of the research work.

travertine thickness, hydrography, groundwater levels, distance to faults, and one precursory factor, i.e. InSAR ground motion rates. These factors, together with the sinkhole inventory map shown in Figure 2, were used as input parameters for producing the sinkhole susceptibility map on the Guidonia-Bagni di Tivoli area. For this elaboration we exploited the *MaxEnt* software package (Phillips et al. 2021).

The factors contribution in the model was computed through some evaluation metrics, i.e. response curve outputs and Jackknife plots of each used environmental variable. An accuracy assessment on the susceptibility map was also performed within *MaxEnt* through empiric receiver operating characteristics (ROC) analysis for examining the precision of the method and its predictive capacity.

Secondly, we collected data on the elements at risk of the study area. These data were derived from the geo-topographical cadastral database of structures and infrastructures at municipal scale distributed by the Lazio Region, merged with the land use map. Thus, this layer includes a classification of properties and facilities exposed to risk according to their nature and functionality. The quantification of the vulnerability was then performed by assigning a percentage of expected damage for each type of element at risk, whereas the economic exposure values were collected from the national real estate market values, to produce the related maps over the whole study area. The integration of the results from the different maps was implemented in a GIS environment and led to the elaboration of the sinkhole risk map of the Guidonia-Bagni di Tivoli area.

3.1. Machine learning algorithm *MaxEnt*

The used machine learning algorithm *MaxEnt* (*Maximum Entropy*) is based on the principle of maximum entropy, as its name implies, for the best approximation of a probability distribution (Jaynes 1957). Entropy, as introduced by Shannon (1948), is defined as the expected value of the self-information of a variable, thus it refers to the amount of information in that variable.

3.1.1. Operating principles and process

The *MaxEnt* model was originally conceived as a general predictive approach in biodiversity studies for modelling presence-only data (that are spatial data where the presence of

an event on a location, if known, is certain, but its absence is not, as it can be due to lacking information) in the species distribution, but it is suitable for all applications involving presence-absence datasets (Phillips et al. 2006). Therefore, the algorithm has been also used as data-driven model for susceptibility mapping of geological phenomena, e.g. landslides (Convertino et al. 2013; Felicísimo et al. 2013; Di Napoli et al. 2020; Javidan et al. 2021).

The MaxEnt model estimates the spatial distribution of an event by finding the distribution that has the highest entropy and that is subject to a series of environmental conditioning factors characterizing the events (Phillips et al. 2006).

In particular, the method compares the probability density functions of each environmental input variable (in our case, the chosen conditioning factors) at the event occurrences (in our case, the sinkhole locations) and at any other location on the study area, and computes the difference as ‘relative entropy’ (Convertino et al. 2013; Kornejady et al. 2017). Then the MaxEnt algorithm analyses the probability density functions of the environmental variables, transformed into logistic values, and finds the one that maximizes the entropy of information, in order to forecast the sinkhole event by spatially mapping its probability to occur, i.e. the susceptibility.

On the Guidonia-Bagni di Tivoli study area, the sinkholes inventory was randomly split into a training set (70% of the total inventory) used for the model itself, and a testing set (30%) employed to validate the predictive capacity of the method.

The MaxEnt algorithm was used by elaborating the average of 6 repeat models and 1000 iterations for each model, in order to tune the system performance and search for the best result. Thus, the result of these elaborations was an average susceptibility map based on six maps each calculated on the result of 1000 iterations. Within *MaxEnt*, the cloglog (complementary log-log regression) logistic model was used (Phillips et al. 2021) and combined with the bootstrapping system (that means that training data are selected by random sampling and by re-entry of the points of presence, so that each point of presence can be sampled many times for each set).

3.1.2. Factor contribution metrics and accuracy assessment

The *MaxEnt* algorithm allowed the calculation of the weights for each class of every conditioning factor used as an environmental variable in the model by means of response curve graphs. In particular, if the variable is continuous, the output is actually a response curve, while if the variable is categorical, the output is a histogram. These graphs show how the probability of predicted presence changes as the value of each environmental variable changes, while keeping all the other variables at their average value.

Furthermore, a jackknife test was performed to further check the contribution of each environmental variable in the model calculation developed by *MaxEnt*. Jackknife is a resampling method that estimates the variability of a statistic from the variability of that statistic across subsamples plot (Sinharay 2010). The Jackknife test removes one variable at time and records the change in the chosen AUC evaluation metric. The plot provides two values for each variable: the first one is the AUC value that would be obtained using only that variable, while the second one is the AUC values obtained considering all the other variables except that one. The importance of the input environmental variables within MaxEnt can be also listed by extracting two metrics named ‘percent contribution’ and ‘permutation importance’. The ‘percent contribution’ values derive from the training process and the particular path that the MaxEnt algorithm uses to get to the best solution: while the MaxEnt model is being trained, it keeps track of which environmental variables are contributing to fitting the model. Each step of the MaxEnt algorithm increases the

gain of the model by modifying the coefficient for a single feature; the software assigns the increase in the gain to the environmental variables that the feature depends on and convert values to percentages at the end of the training process providing ‘percent contribution’ for each variable (Phillips et al. 2006). The ‘permutation importance’ of each variable depends only on the final MaxEnt model, not the path used to obtain it: for each environmental variable in turn, the values on training presence and background data are randomly permuted. The model is re-evaluated on the permuted data, and the resulting decrease in training AUC is computed and normalized to percentages. A large decrease indicates that the model depends heavily on that variable (Phillips et al. 2006).

The accuracy assessment of the produced sinkhole susceptibility map implies the evaluation of the finest combination map from the processed tests within *MaxEnt* and was performed by empiric ROC analysis and cross-comparison of the area under curve (AUC) values.

3.2. Conditioning and precursory factors for sinkhole susceptibility

According to the most representative morphological and spatial features of the study area with regard to sinkhole phenomena, we selected the eight conditioning and precursory factors. All the factors, either classified as categorical or numerical discrete data, were computed as thematic layer with the same 10 m cell-size to be used as input data for *MaxEnt*. In particular, those categorical data (lithology, land use, hydrography) that contain a finite number of categories were rasterized. Those maps that contain a spatially discontinuous information (i.e. point-wise and counter-lines maps) were spatially interpolated to obtain a continuous thematic layer: more in detail, such vectorial linear elements (faults, groundwater, soft soil and travertine thickness lines) and point-like elements (ground motion rates of InSAR benchmarks) were converted into continuous surface maps by means of the Inverse Distance Weighted tool in GIS environment (Figure 4).

3.2.1. Lithology

Lithology is an intrinsic factor in the problem of sinkholes as these phenomena preferentially occur in specific lithological situations that involve soluble rocks. Thus, the lithotype data can provide indications in advance about possible locations of sinkhole formation. The geolithological map of the Guidonia-Bagni di Tivoli study area was collected from Lazio Region authority (Figure 4). The lithotypes cropping out in the area have been grouped into 10 lithological classes. The most representative lithology is the travertine that outcrops in the central portion of the area and extends up about 20 km² (nearly 70% of the whole basin).

3.2.2. Land use

The land use map of the study area, derived from merging levels 2 and 3 of the CORINE Land Cover map (European Environment Agency 2007), shows that croplands and semi-natural zones cover most of the study area (Figure 4). The travertine quarry area currently extends over an area of about 4 km². The most significant built-up zones of the study area correspond to Collefiorito, Guidonia-Montecelio, Bagni di Tivoli, Villalba and Villanova villages.

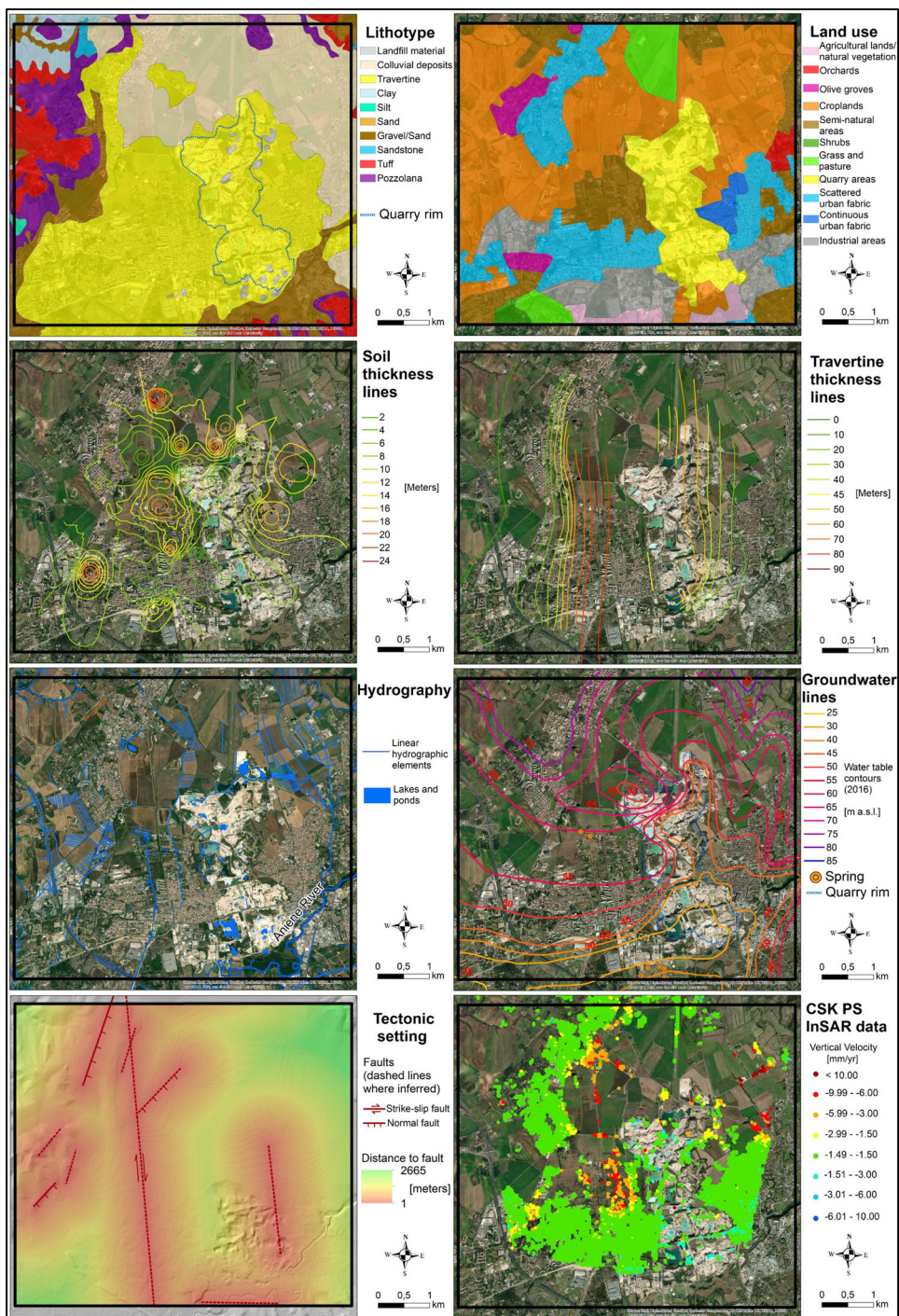


Figure 4. Maps of the eight conditioning and precursory factors chosen for assessing the sinkhole susceptibility over the study area. These maps are referred to the categorical and discrete data as they were available over the study area. Then, all the factor maps were converted into continuous surface raster maps with the same 10 m cell-size to be used as input data for MaxEnt algorithm.

3.2.3. Soft soil thickness

Soft soils correspond to compressible recent alluvial deposits that constitute the terrain surface layer throughout the plain. Data referred to the thicknesses of these soils were obtained from (Bozzano et al. 2015), who showed that the thickest stratigraphical layers correspond to the areas affected by the highest rates of ground lowering, due to water pressure decrease and consolidation processes (Figure 4).

3.2.4. Travertine thickness

The thickness of the travertine in the area was reproduced as discontinuous thickness contour lines derived from the work of Faccenna et al. (2008), who created a travertine thickness map by interpolating data of 114 boreholes. The map shows that the highest thickness is in the center of the study area (up to 90 m) and inside the quarry area, and decreases moving away from them (Figure 4).

3.2.5. Fault setting

The main N-S striking fault beneath the Acque Albule basin has a right-lateral strike-slip kinematics and is partly covered by the travertine plateau. Other associated faults are NE-striking with an oblique to normal kinematics and other inferred or blanketed minor tectonic discontinuities (Gasparini et al. 2002; Faccenna et al. 2008; Rinalduzzi et al. 2017). The used thematic layer for the structural setting of the study area is the spatial distance from faults (in meters) represented as an interpolated continuous surface map (Figure 4).

3.2.6. Hydrography

In the Guidonia-Bagni di Tivoli plain, the surface hydrographic network is poorly developed, probably for the presence of a well-developed sub-surface karst network in the Pleistocene travertine deposit. Many relict sinkholes are presently lakes. The Aniene River is the major hydrographic feature in the area, as it drains the majority of surface and sub-surface waters (Rinalduzzi et al. 2017). The map of the surface hydrographic network of the study area was obtained from Lazio Region authority (Figure 4).

It is worth stating that hydrographic data were managed as categorical data: indeed, in this case, before converting data into a raster layer, the map was transformed into a matrix of presence-absence of the hydrographic element with an applied buffer of 50 m, without generating a map of the distances from the element since the effect of hydrography is much more limited around the element itself.

3.2.7. Groundwater

The piezometric data were taken from the most recent available cartography of Guidonia-Montecelio municipality that dates back to 2016 (Figure 4). The water table contour lines displayed refer to the depth to groundwater of the shallow aquifer from ground level in meters above sea level. Despite the huge deep water recharge, the shallow aquifer is characterized by cone of depression due to water abstraction in the travertine mining area, where a strong distortion of the contour lines induced by the quarrying-related dewatering activities is evident (De Filippis et al. 2013). Several geothermal springs and gas venting structures are present in the area, mainly located along the tectonic discontinuities (Faccenna et al. 2008; Brunetti et al. 2013).

3.2.8. Satellite InSAR data

Satellite PSI (Persistent Scatterer Interferometry) InSAR data are point-wise ground deformation measurements extracted through the processing of a long temporal data stack

of remotely sensed SAR images acquired by space-borne systems (Crosetto et al. 2016). The analysis of ground movements revealed by PS (Persistent Scatterers) radar benchmarks in terms of spatial and temporal patterns of velocity (mm/year) can support the evaluation of subsidence rates with millimetric accuracy over time.

On the Guidonia-Bagni di Tivoli study area, the available PSI ground deformation data derive from 274 SAR images acquired in X-band in both orbits (ascending and descending) by COSMO-SkyMed (ASI, Italian Space Agency) constellation in the span time 2017–2020 and processed through the CPT (*Coherent Pixel Technique*) approach (Mora et al. 2003). The PSI yearly average velocities measured along the satellite LOS (Line Of Sight) were decomposed into their horizontal and vertical components, by following procedures proposed by Notti et al. (2014). The decomposition revealed a main vertical direction of displacement with a negligible horizontal component, as already indicated by past works in the study area (e.g. Bozzano et al. 2015). The map of vertical movements provides subsidence rates from 10 to 20 mm/year located in the central part of the study area and referred to human-made structures and infrastructures (Figure 4).

3.3. Elements at risk (EAR) exposure and vulnerability

The EAR exposure and sinkhole vulnerability maps over the Guidonia-Bagni di Tivoli plain were derived from cadastral and topographic databases and from market income values, as well as from bibliography.

Information on the size (diameter) of sinkholes on the study area was missing since the inventoried sinkholes used for the predictive model almost exclusively consist of point-like data. Thus, the empirical intensity of sinkholes based on their average diameter could not be considered. Therefore, it was assumed that the impact of a sinkhole on structure/infrastructure would highly damage the economic productivity and serviceability, regardless of the collapse diameter.

Hence, the vulnerability to sinkholes over the study area was derived by solely considering the type of the different Elements At Risk (EAR). In this perspective, the vulnerability map indicates the degree of expected economic and human losses due to sinkhole activity in each portion of the territory, by considering the ‘strategic’ usability of exposed EAR, as defined by Solari et al. (2018).

The vulnerability map in the Guidonia-Bagni di Tivoli area was constructed by assigning values to different EAR based on the identification of the areas and structures where sinkhole-related direct and indirect damage is expected to reach higher values.

Firstly, the EAR catalogue of the study area was collected from national geo-topographic databases which contain information about private buildings, economic and industrial activities, public service utilities and infrastructures. This catalogue only includes simple information about the location and the type of the structures: neither the structural state, maintenance status, construction type nor human occupancy of buildings were available. This vector database (DB) of buildings and linear elements (road network or other transportation paths) was merged with the polygons of the second-level CORINE Land cover map to classify the EAR types. Thus, the quantification of the vulnerability was performed by assigning a percentage of expected damage to the EAR, for each type of element at risk. The vulnerability values were chosen according to various classifications already proposed in the scientific literature for geohazards (usually for landslide events) (Catani et al. 2005; Papathoma-Köhle et al. 2007; Bianchini et al. 2017; Solari et al. 2018).

The exposure of the EAR refers to the monetary value, i.e. the price or current value of the asset, to be based on potentially lost earnings. These values were extracted from the Italian OMI (*Osservatorio Mercato Immobiliare* – Real Estate Market Observatory) database; the real estate quotas identify, for homogeneous territorial area of each Italian municipality, a minimum and maximum range of the average market and rental values, per unit of surface area in euro per m², by type of property and state of conservation for residential buildings. In addition, an exposure value was also assigned to all the other structures, road network and areas of the CORINE land cover map, according to web bibliographic values (e.g. Catani et al. 2005; Pellicani et al. 2014; Perino et al. 2018) and to the ‘Average Agricultural Values’ derived from the OMI database that contain an estimate of the value in €/ha of agricultural land referred to the year 2020, in order to assign exposure value to all the assets of the area.

3.4. Sinkhole risk map

The sinkhole risk map over the study area was computed in GIS environment by the combination of the three component rasterized maps, i.e. susceptibility, exposure, and vulnerability, with the same 10m cell-size resolution. In particular, the three layers were combined by using the Raster Calculator tool of ArcGIS, based on the formula of Risk ($\text{Risk} = \text{Susceptibility} * \text{Vulnerability} * \text{EAR Exposure}$) in its strict sense.

The sinkhole risk map was classified and grouped into five classes (‘very high’, ‘high’, ‘moderate’, ‘low’, ‘very low’) for visual interpretation by using natural intervals classification in GIS environment (Jenks 1989).

4. Results

4.1. Susceptibility zoning map

The sinkhole susceptibility map of the study area was produced as *MaxEnt* output map (Figure 5a). The map is a 10m cell-size raster layer with continuous values from 0 to 1. The most susceptible areas are located south of Guidonia-Montecelio village, NE of Villalba village, in the central area of the travertine quarry area, and in the semi-natural area in the SW edge of the study area, W of Bagni di Tivoli village (Figure 5a).

Regarding the accuracy assessment of the modeled susceptibility map, the AUC value for the testing data is 0.857, demonstrating a good prediction ability of the model (Figure 5b).

Regarding the response curves of the eight conditioning and precursory factors used as environmental variables in the model (Figure 5c), the response curve of lithology shows that the travertine reveals the highest relative weight since the presence of potentially karstic rock is an essential requisite for the development of dissolution-induced sinkholes. The other two most relevant lithologies are pozzolana and colluvial deposits. The first one is important because it is not very widespread on the study area, but it outcrops close to areas with a high density of sinkholes; the second one, in addition to being the most widespread lithology in the area after travertine, it is also deposited on it and therefore could collapse due to the underlying travertine. This results also demonstrates the effectiveness of the model to represent well the input data in/close to the sinkhole areas.

The land cover/use classes that mostly influence the predictive model are the quarry areas and the continuous urban fabric. This latter land-use class shows a reduced areal extension, but a high mapped sinkholes density. The high weight of this factor could be

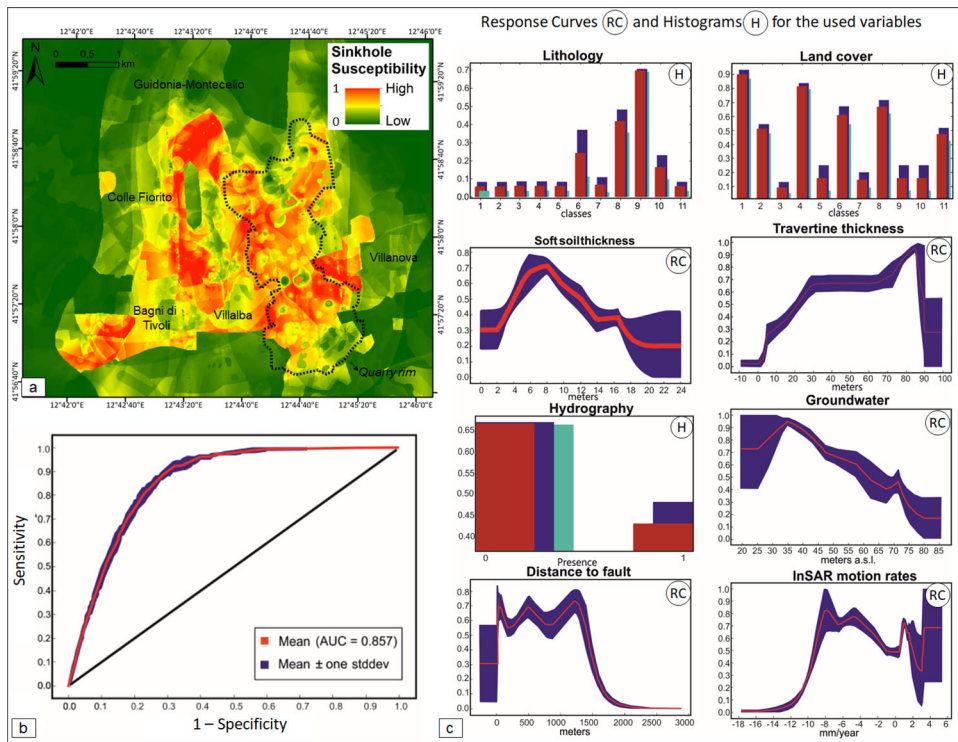


Figure 5. (a) Sinkhole susceptibility map of the study area; (b) AUC value of the ROC analysis (stddv = standard deviation); (c) Response curves (RC) and histograms (H) for the used variables. In RC, the red line represents the average value of the computed six repeats of the test, the blue area shows the average value \pm stddv. The light blue bar represents the model without the variable. The blue bar represents the model with the only variable. The red bar represents the final output. (Lithology classes: 1 = Landfill; 2 = Clay; 3 = Sand; 4 = Tuff; 5 = Silt; 6 = Lithic tuff; 7 = Pozzolana; 8 = Colluvial deposit; 9 = Travertine; 10 = Gravel/Sand; 11 = Sandstone; Land use classes: 1 = Continuous urban fabric; 2 = Scattered urban fabric; 3 = Industrial areas; 4 = Quarry areas; 5 = Orchards; 6 = Olive groves; 7 = Grass and pasture; 8 = Agricultural areas; 9 = Cropland; 10 = Scrubs; 11 = Semi-natural areas.).

related to the easier evidence of a sinkhole occurred on built-up populated areas where it can be effortlessly observed and reported.

The response curve of the soft soil thickness shows that the spatial likelihood of sinkholes decreases where thickness is higher than 8–10 m, indicating that the cover thickness should be relatively thin, since cavities rooted in the travertine bedrock have to propagate upwards to reach the surface and produce a sinkhole. Conversely, the travertine thickness is a key factor especially where thickness is higher, i.e. up to 70–85 meters. This is confirmed by comparing the susceptibility map with the travertine thickness map (Figures 4 and 5a), since an abrupt increase of the susceptibility value is noticed in correspondence to the maximum thickness values (i.e. higher than 80 m).

The hydrography histogram divides the result into the water body presence (value 1) or absence (value 0), being the latter one referred to higher susceptible ranges even if output seems to be not very clear. Concerning the response curve of groundwater levels, lower values turn out to be more relevant for sinkhole susceptibility since shallow levels entirely lie in the susceptible travertine layer while deeper levels lie in the Plio-Pleistocene or Mesozoic deposits.

The distance to fault seems to be influential for sinkhole susceptibility within a range of one kilometer, whereas beyond this threshold the weight of the parameter promptly

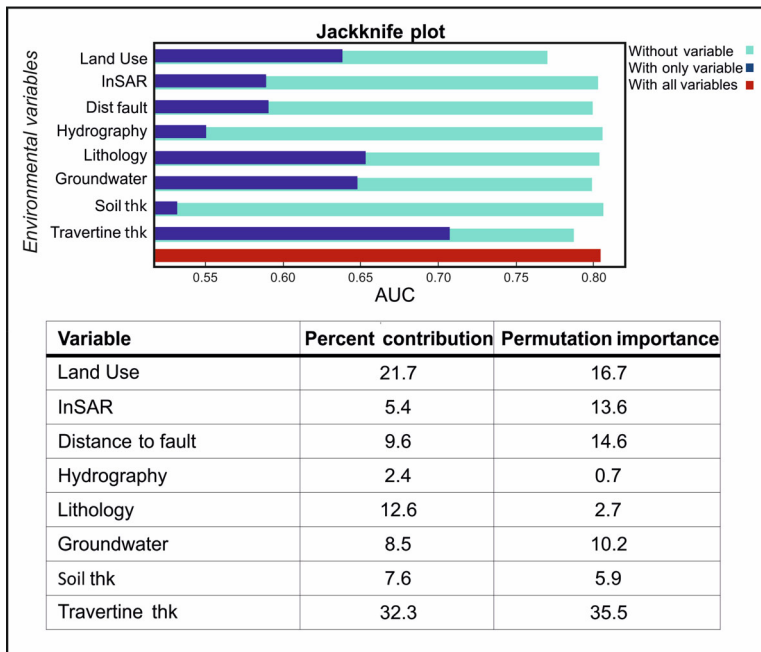


Figure 6. Jackknife plot for the used environmental variables. Used abbreviations: thk = thickness; dist fault = distance to fault. Colored bars: The light blue bar represents the AUC of the model without the corresponding variable. The blue bar represents the AUC processed with only the corresponding variable. The red bar represents the AUC of the final model using all the variables.

decreases in the model. This is because fault zones in travertine and carbonate rocks are commonly characterized by higher hydraulic conductivity and may act as preferential pathways for geothermal fluids that may increase groundwater aggressiveness.

InSAR ground motion rates show poor correlation with potential sinkhole development: the response curve is quite noisy, even if it records a peak for vertical velocities between -10 and -5 mm/year. Basically, the deformation measured by satellite radar data confirmed the subsiding movements historically reported in the area even by past InSAR data (Nisio et al. 2007; Ciotoli et al. 2016; De Ritis et al. 2020).

By observing the jackknife histogram plot and the summary table of the eight used variables, and by considering both the AUC values ‘with only variable’ and ‘without variable’, the results of the jackknife test show that the most determining factors are the lithology, the travertine thickness, groundwater and the land use, whereas soft soil thickness and the hydrology represent the least important factors for the calculation (Figure 6).

The range of continuous values of the sinkhole susceptibility map has then been divided into five classes of susceptibility (very low, low, medium, high, very high) by using the natural breaks method. This classification was made to enable the cross-comparison of the susceptibility map with the sinkhole inventory and to compute statistics of mapped sinkhole locations in each susceptibility class. The resulting outcomes demonstrate the good predictive ability of the used model (Figure 7). In particular, out of 202 total sinkholes present in the area, an amount of 95 occurrences falls into the areas classified with Very High sinkhole susceptibility (about 47%) and 71 occurrences fall into the high susceptibility class (about 35%). 23 sinkholes, corresponding to 11% of the total, fall into the medium susceptibility class, while the remaining 7% is divided into Low or Very Low susceptibility classes (Figure 7).

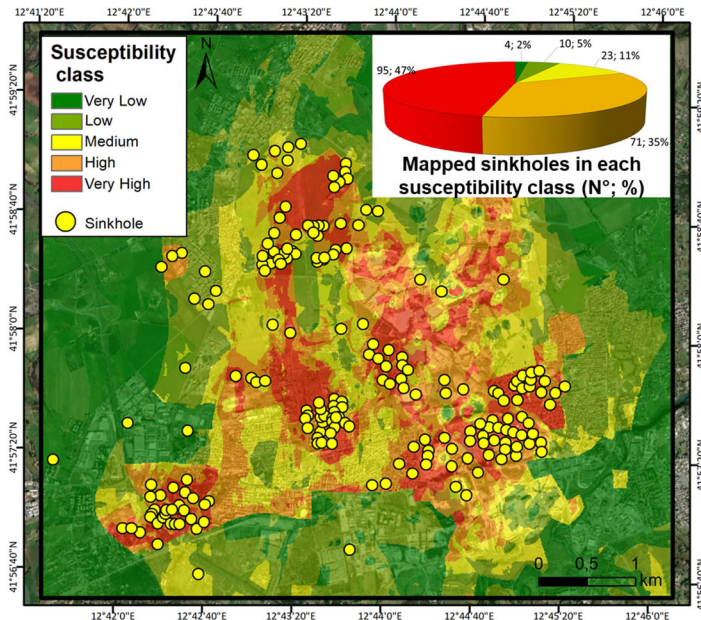


Figure 7. Sinkhole database overlapped on sinkhole susceptibility map. Pie chart of the number and percentage of mapped sinkholes in each susceptibility class.

4.2. Vulnerability and exposure of elements at risk

The sinkhole vulnerability intended as the expected degree of damage due to sinkhole impact on human elements was computed and produced as a map over the Guidonia-Bagni di Tivoli plain (Figure 8).

The proposed vulnerability map in the Guidonia-Bagni di Tivoli area (Figure 8b) includes different values of expected economic and human losses due to sinkholes assigned to different EAR (Figure 8a) on the territory. In particular, by taking into account the importance within society and usability of exposed EAR to sinkhole events, the higher percentages of expected damage were assigned to strategic structures that would contain population (e.g. hospitals, schools, residential buildings). High vulnerability values were also assigned to the roads and road internal network by bearing in mind the significant indirect impact in functionality loss on transportation paths produced by potential sinkhole (Table 1).

The exposure of the EAR referred to the monetary value over the study area includes 7 real estate value classes of OMI zonation over the study area used for the EAR exposure calculation of residential buildings, with values ranging from around 1200 €/m² to around 1600 €/m² (Figure 8c). The other exposure values derived from the OMI database or web bibliographic values assigned to all the other structures were lower, e.g. areas of the CORINE land cover map, up to a minimum value of 0.2–50 €/m² range class for the agricultural and semi-natural areas. The output of this merging procedure is a continuous rasterized exposure value map over the whole study area (Figure 8d).

4.3. Risk assessment map

The output sinkhole risk map on the Guidonia-Bagni di Tivoli study area is a raster surface with 10-m cell size resolution based on five classes of risk, named very low, low, medium, high, and very high (Figure 9).

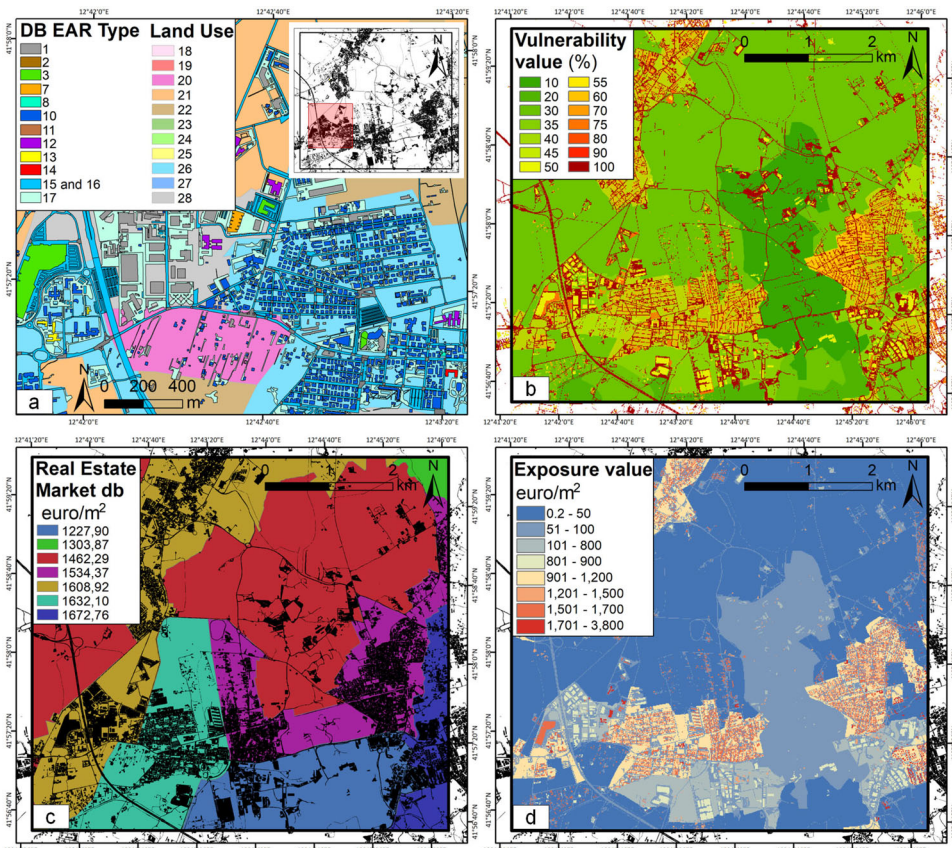


Figure 8. (a) Close-up of the study area that shows the map of EAR type. Numbered EAR and Land Use types refer to Table 1; the up-right box shows the location of the close-up; (b) Sinkhole Vulnerability map of the study area; (c) Zonation and values (€/m²) of OMI Real Estate database; (d) Exposure value (€/m²).

Overall, it can be noted that the mapping of areas with higher risk (High and Very High risk classes) covers about 2% of the total study area and primarily relies on the zoning of the main urban fabric, since both the potential damage (the product of vulnerability and EAR exposure) and the susceptibility pivot on the land use and thus on the built-up area distribution. The Medium Risk class encompasses a percentage of about 3% of the total study area, whereas 89% refers to the Very Low risk class.

Basically the risk is higher in the most susceptible and vulnerable urbanized areas, i.e. in the Villanova, Bagni di Tivoli and Villalba villages, whereas it decreases in areas characterized by lower susceptibility and vulnerability. In particular, it is worth to highlight that 5% of the whole road-network pavement (including roads and internal roads) and 27% of all the residential buildings fall into High and Very High risk classes.

In particular, the numbers of manufacts of different functional type characterized by different risk values were computed (Table 2): for these statistics we assigned a risk class value to each manufact by considering the spatial majority of cell values of the risk class that fall into the manufact.

It is worth to highlight that, besides 484 residential buildings in Very High Risk Class and 985 in High Risk Class, some strategic structures of social and collective relevance are also located in areas of High and Very High Risk, i.e. five schools, one administrative building, two religious complexes, one social security edifice and one touristic complex.

Table 1. Vulnerability values in percent for each element at risk (EAR) type.

DB EAR type		Vulnerability value (%)
1	Industrial building	50
2	Parks and sport centers	50
3	Commercial building	50
4	Agricultural stable and breeding farm	50
5	Airport station	55
6	Railway station	55
7	Cultural and media-related building	60
8	Church/Religious complex	60
9	Public/administrative building	60
10	Residential building	75
11	Social security edifices	60
12	Schools	80
13	Hospitals and health centers	90
14	Touristic complex	70
15	Parking areas	80
16	Roads	100
17	Internal road network	100
Corine land cover		Vulnerability value (%)
18	Agricultural land with significant areas of natural vegetation	10
19	Orchards	40
20	Olive groves	40
21	Croplands	20
22	Semi-natural areas	20
23	Shrubs	10
24	Grass and pasture	30
25	Quarry areas	10
26	Scattered urban fabric	45
27	Continuous urban fabric	45
28	Industrial areas	35

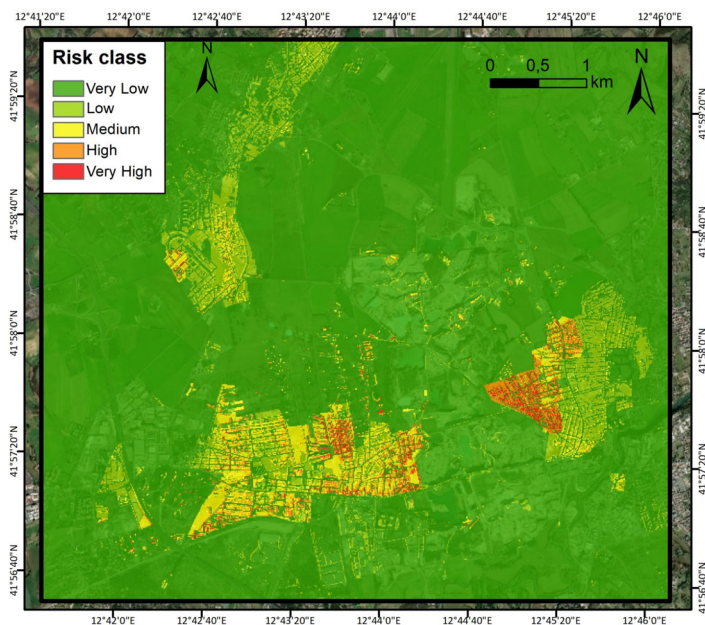
**Figure 9.** Sinkhole Risk map of the study area.

Table 2. Number of manufacts of each EAR type in each risk class.

DB EAR type	Very Low	Low	Medium	High	Very High
1 Industrial building	294	84	56	2	0
2 Parks and sport centers	0	3	4	2	0
3 Commercial building	2	0	2	0	0
4 Agricultural stable and breeding farm	5	0	0	0	0
5 Airport station	5	0	0	0	0
6 Railway station	1	1	0	0	0
7 Cultural and media-related building	2	0	1	0	0
8 Church/Religious complex	2	4	2	2	0
9 Public/administrative building	0	0	0	1	0
10 Residential building	1296	1858	1196	985	484
11 Social security edifices	0	0	0	1	0
12 Schools	2	4	6	4	1
13 Hospitals and health centers	2	0	1	0	0
14 Touristic complex	1	0	0	0	1
15 Parking areas	439	0	0	0	0

5. Discussion

In this work, the sinkhole risk assessment on the Guidonia-Bagni di Tivoli area was performed through the evaluation of each risk sub-component, i.e. susceptibility, vulnerability and exposure of the subjected elements at risk.

The Guidonia-Bagni di Tivoli plain is a well-known sinkhole area with outcropping Plio-Pleistocene marine sediments, volcanic deposits and thermogenic travertine. It is a typical multi-hazard scenario, with extensive cases of subsidence and historical occurrence of sinkholes filled with ground and regolith under the load of multi-story buildings in a geothermal-seismic setting. Nevertheless, to our knowledge, a comprehensive sinkhole risk map had not been produced yet.

In such an area, characterized by hidden sinkholes or similar karst structures in the shallow subsurface of densely populated surface, a sinkhole risk map is a useful tool to manage or at least assess this environmental source of hazard. In particular, it can help to understand the spatial distribution and dynamics of sinkhole phenomena and hopefully to forecast their occurrence, particularly in the parts of the basin where active movements have caused damages to buildings and infrastructures.

The first important step in sinkhole risk analysis is the construction of a comprehensive cartographic sinkhole inventory. Sinkhole databases should include information on the location of sinkholes limits, chronology, morphometric parameters, and underlying structures (Gutiérrez et al. 2014; Kleinhans and Van Rooy 2016). Sinkhole inventory seems to be a primary data source in training the model. In this work we rely on previously mapped sinkholes from bibliographic data sources (ISPRA database and previous works, i.e. Billi et al. 2016) and we manage the sinkhole occurrence as point-like location data. This has decreased the detail of the analysis, but it was considered both necessary as input data for *MaxEnt* model, and reasonable when working over large area. Moreover, since chronological information was not available on all the inventoried sinkholes, then the sinkhole hazard has been represented by a sinkhole susceptibility, which only identifies areas potentially affected by phenomena and does not imply an occurrence time or frequency for the events (Dai et al. 2002; Galve et al. 2011). A relevant future perspective could include on-site investigation on the study area to search for present in-situ evidence and thus a fieldwork could be required to identify current sinkholes as lacking in this research that only considers already mapped past sinkholes derived from literature.

The sinkhole susceptibility assessment was performed by means of maximum entropy algorithm through the *MaxEnt* model. This machine learning algorithm is a data-driven

model that has been already used for geohazard susceptibility mapping and that has revealed its effectiveness. In scientific literature it has been compared with various other modeling and has been evaluated as an excellent predictive approach, since it provides a continuous distribution model and has a very stable confidence interval system (Phillips et al. 2006; Townsend Peterson et al. 2007; Kaky et al. 2020). The *MaxEnt* approach is based upon a probabilistic framework and in our work was chosen with the purpose of using a machine learning algorithm that generates predictions from an incomplete set of information. The *MaxEnt* algorithm is a presence-only model, exploited where presence data are abundant, but absence data are hard to obtain and often unreliable due to insufficient survey effort. To counter the lack of absences, *MaxEnt* uses a background sample to contrast the distribution of presence data along environmental gradients against the distribution background points, randomly drawing from the study area (Gomes et al. 2018).

The limitation of this open-source tool of managing only point-wise data was, in our case, aligned with the lack of information concerning the actual size of the sinkhole events. Several conditioning and causative factors for the observed historical sinkhole occurrence and subsidence have been considered in the Guidonia-Bagni di Tivoli study area. Results of susceptibility modelling show that the presence and the thicknesses of travertine, as well as the distance to fault and the groundwater exploitation are the main causal factors for sinkhole occurrence and outline a physical understanding of sinkhole formation in the study area. In particular, the importance of the different causal factors has been highlighted through the analysis of the resulting sinkhole susceptibility map and jackknife tests. Such graphs clearly indicate the relevant role of two environmental variables, i.e. the lithology and the thickness of the travertine, which are inter-correlated parameters. The most susceptible areas to sinkholes are found in correspondence to the maximum travertine thickness values, i.e. higher than 80 m, and where soft soil thickness is thin since this situation can facilitate the upward propagation of cavities within travertine bedrock. This is also in agreement with other studies of geomechanical modelling that analyzed the conditions of sinkhole formation depending on the rock mechanical parameters, cover thickness and depth of solution zone (e.g. Kleinhans and Van Rooy 2016; Al-Halbouni et al. 2019). It is worth to highlight that ground collapses are influenced not only by lithology, i.e. travertine, but actually by the rock mechanical conditions. In this regard, previous works (De Ritis et al. 2020) carried out detailed geophysical-geotechnical studies on the area, and correlated ground surface variations (undulations, small sinkholes and fractures) with the presence of disarticulated travertine blocks in the stratigraphical sequences.

The presence of fault systems also plays a relevant role for facilitating the water circulation and thus the propagation of collapse phenomena. In particular, tectonic discontinuities coupled with the poor rock mechanical characteristics could increase the upward migration of *deep piping sinkholes* from the triggering point towards the soil surface, as also demonstrated in scientific literature (Caramanna et al. 2008).

Secondarily, also the land use classes of quarry areas and the continuous urban fabric turns out to be a relevant conditioning factor in sinkhole susceptibility mapping on the study area. This could be related to the easier evidence of a sinkhole occurred on urbanized areas, but it is also in agreement with previous works on sinkhole formation on the Guidonia-Bagni di Tivoli basin (e.g. Brunetti et al. 2013; Bozzano et al. 2015) which pointed out that the continuously growing urbanization with related overloads, as well as groundwater pumping due to anthropic causes (e.g. the travertine quarry activities, thermals spa, and several agricultural and domestic wells) are among the main sinkhole causal

factors in the area. This facet underlines the problem of the urban development above sinkholes, which were obliterated by buildings at the time of construction but could determine new subsidence with the overloading.

Groundwater is also a relevant parameter for sinkhole potential occurrence. In particular, the water pumping accelerates groundwater flow in the areas affected by cones of depression and causes drainage of karst conduits. Moreover, the thermal aggressive groundwater in fractured and karstified travertine would favor dissolution and bottom-up erosion processes and would reduce the mechanical strength and bearing capacity. However, not all data on water exploitation are available, since some wells are not notified to the Environmental Local Authorities, so a complete quantification of these water amount is not possible. From this point of view, even other hydrogeological factors may play a significant role in sinkhole development, including aquifer permeability, transmissivity, flow direction, etc., but we did not take in account these kinds of information in our work because comprehensive data are missing, so we consider this aspect as a constant in the whole study area.

The slow-moving ground deformations estimated by InSAR data confirmed the vertical downward movement already documented in the area. These data could not monitor the rapid sinkhole occurrence due to the intrinsic limitations of interferometric techniques, but could be likely correlated to downward gravitational movement of the overlying material or to an incipient vast ground sinking related to compaction or a larger karst depression (e.g. Intrieri et al. 2018; Nof et al. 2013; Esposito et al. 2021).

In terms of vulnerability and potential damage, it is worth highlighting that the sinkholes may cause both direct and indirect losses. For instance, when a sinkhole occurred on a transportation infrastructure, the direct damage corresponds to the injuries caused by the event and by the cost of repairing or reconstructing the road. On the other hand, the indirect losses (i.e. the impact on the economic productivity caused by the temporal loss in serviceability, or resulting delay in the transportation of people and goods), although difficult to estimate, are frequently higher than the direct ones (Gutiérrez et al. 2014). The maps of vulnerability and EAR exposure value related to sinkhole events over the study area were based on quite accurate and updated values derived from different sources with different detail and scale, i.e. geo-topographic databases, real estate market databases, bibliographic information. On one hand, the exploitation of accurate and updated values from the real estate market database that includes quotas in €/m² of the average market and rental values of buildings, as well as current Average Agricultural Values permitted to reach fine exposure values for assessing the potential damage over the study area. An economic exposure value was specifically assigned to the road network according to bibliographic data on construction or renovation costs of regional and local roads (Pellicani et al. 2014; Solari et al. 2018). Also, we assumed the highest impact of a sinkhole event on structure/infrastructure in terms of serviceability loss, regardless of the collapse diameter. On the other hand, in our work the intensity of sinkholes was not computed due to missing information about the sizes of mapped collapses, and it was assumed as maximum for all the phenomena. Likewise, in this work the available EAR database only includes simple information about the type of structures over the study area: neither the structural state of the manufactures nor data about the occupancy of buildings were available at this working scale. More accurate and complete data on the geometrical dimensions (diameters, depths) of sinkholes and on the characteristics of buildings and inhabitants surely would permit to compute the vulnerability more objectively, and overall should be better tackled within the sinkhole risk evaluation practices.

Once the sinkhole risk map is generated, various methods for map classification exist and are available within GIS software such as natural breaks, equal interval, equal area, quantiles, geometrical interval, standard deviation. They are chosen depending on the conditions and distribution of the specific data population over the study area. For instance, the equal intervals or equal area classification methods work reasonably well on data that are normally distributed, while the quantile classification is more applicable for positive or negative skewed data. The natural breaks method divides the classes for grouping similar values and maximizing the differences, so that class boundaries are placed where the greatest difference between classes is found. Accordingly, in this work the classification of sinkhole risk was applied by using natural breaks (Jenks 1989), in order to avoid polarising the data. The same approach has been commonly used in similar studies on sinkhole susceptibility and risk mapping (e.g. Yilmaz 2007; Taheri et al. 2015).

Risk maps can vary, depending on the data layers that are inserted. Overall, over the Guidonia-Bagni di Tivoli study area the sinkhole risk assessment map that relies on the computed susceptibility, vulnerability and exposure, reaches up a reasonable precision thanks to the suitable cartography used for EAR structures and infrastructures, and highlights the critical areas related to the continuous urban fabric, and lower values of specific risk in areas classified as highly susceptible but without vulnerable elements. As a result, the sinkhole risk map displays the most significant sinkhole-prone areas to be monitored and controlled in order to avoid damage to population and structures, and thus can support urban planning and environmental management strategies at a municipal scale.

6. Conclusions

Sinkhole occurrence, especially in urbanized areas, is a major hazard that can cause significant economic and social damage in terms of losses and injuries to services, structures and infrastructures. In this work we presented a sinkhole susceptibility and risk assessment mapping in Guidonia-Bagni di Tivoli plain, near Rome, in Central Italy where sudden sinkholes have historically and recently occurred.

We took into consideration a simple point-like sinkhole database from literature due to lacking data about depth and size of mapped collapses and a series of environmental sinkhole-conditioning factors on the study area. A sinkhole susceptibility map was produced by means of maximum entropy algorithm through *MaxEnt* model. Results of the study reveal that the presence and thicknesses of travertine, the presence of faults and the groundwater exploitation are the main causal factors for sinkhole occurrence in the Guidonia-Bagni di Tivoli area. Also the land use classes of quarry areas and continuous urban fabric turns out to be a relevant conditioning factor in sinkhole susceptibility mapping.

The sinkhole risk map of the study area was classified into five risk classes (Very low, Low, Medium, High, Very high) and it reveals that areas within the two higher ones cover up nearly 2% of the total area and primarily relies on the zoning of the main urban fabric (Villanova, Bagni di Tivoli and Villalba villages). In particular, a percentage of 27% of all the residential buildings of the area and 5% of the whole road-network pavement fall into High and Very High risk classes. The Medium risk class of the sinkhole risk zonation map covers a percentage of about 3% of the Guidonia-Bagni di Tivoli study area, whereas 89% refers to the Very Low risk class.

Overall, the outcomes of the work show the development of sinkhole risk mapping in the study area by quantitatively assessing the main sinkhole controlling factors and sinkhole susceptibility throughout the machine learning *MaxEnt* model, even with basic input

data, and by evaluating in GIS environment the associated risk as a useful tool for urban planning and risk management purposes.

Acknowledgements

COSMO-SkyMed SAR images were processed by SINTEMA Engineering srl, Spin-Off Federico II University of Napoli, 80138 Napoli NA, (Italy) by means of PS-like approach technique using coherent pixels technique (CPT) algorithm.


Disclosure statement

No potential conflict of interest was reported by the authors.

Funding

The work was funded by the project ‘MOSCAS – Modelli e Strumenti per la Caratterizzazione delle cavità Sotterranee’ financed by the former Italian Ministry for Environment, Land and Sea Protection of Italy (Ministero dell’Ambiente e della Tutela del Territorio e del Mare – MATTM), now named Ministry of the Ecological Transition.

ORCID

Silvia Bianchini  <http://orcid.org/0000-0003-2724-5641>
 Pierluigi Confuorto  <http://orcid.org/0000-0003-4291-4604>
 Diego Di Martire  <http://orcid.org/0000-0003-0046-9530>
 Domenico Calcaterra  <http://orcid.org/0000-0002-3480-3667>

References

- Al-Halbouni D, Holohan EP, Taheri A, Watson RA, Polom U, Schöpfer MPJ, Emam S, Dahm T. 2019. Distinct element geomechanical modelling of the formation of sinkhole clusters within large-scale karstic depressions. *Solid Earth*. 10(4):1219–1241.
- Al-Halbouni D, Watson RA, Holohan EP, Meyer R, Polom U, Dos Santos FM, Comas X, Alrshdan H, Krawczyk CM, Dahm T. 2021. Dynamics of hydrological and geomorphological processes in evaporite karst at the eastern Dead Sea – a multidisciplinary study. *Hydrol Earth Syst Sci*. 25(6):3351–3395.
- Ammirati L, Mondillo N, Rodas RA, Sellers C, Di Martire D. 2020. Monitoring land surface deformation associated with gold artisanal mining in the Zaruma City (Ecuador). *Remote Sens*. 12(13):2135.
- Argentieri A, Carluccio R, Cecchini F, Chiappini M, Ciotoli G, De Ritis R, Di Filippo M, Di Nezza M, Marchetti M, Margottini S, et al. 2015. Early stage sinkhole formation in the Acque Albule basin of central Italy from geophysical and geochemical observations. *Eng Geol*. 191:36–47.
- Bianchi Fasani G, Bozzano F, Cardarelli E, Cercato M. 2013. Underground cavity investigation within the city of Rome (Italy): a multi-disciplinary approach combining geological and geophysical data. *Eng Geol*. 152(1):109–121.
- Bianchini S, Del Soldato M, Solari L, Nolesini T, Pratesi F, Moretti S. 2016. Badland susceptibility assessment in Volterra municipality (Tuscany, Italy) by means of GIS and statistical analysis. *Environ Earth Sci*. 75(10):1–14.
- Bianchini S, Solari L, Casagli N. 2017. A GIS-based procedure for landslide intensity evaluation and specific risk analysis supported by Persistent Scatterers Interferometry (PSI). *Remote Sens*. 9(11):1093.
- Billi A, De Filippis L, Poncia PP, Sella P, Faccenna C. 2016. Hidden sinkholes and karst cavities in the travertine plateau of a highly-populated geothermal seismic territory (Tivoli, central Italy). *Geomorphology*. 255:63–80.
- Bozzano F, Esposito C, Franchi S, Mazzanti P, Perissin D, Rocca A, Romano E. 2015. Understanding the subsidence process of a quaternary plain by combining geological and hydrogeological modelling with satellite InSAR data: the Acque Albule Plain case study. *Remote Sens Environ*. 168:219–238.

- Brunetti E, Jones JP, Petitta M, Rudolph DL. 2013. Assessing the impact of large-scale dewatering on fault-controlled aquifer systems: a case study in the Acque Albule basin (Tivoli, central Italy). *Hydrogeol J.* 21(2):401–423.
- Buttrick D, Van Schalkwyk A. 1998. Hazard and risk assessment for sinkhole formation on dolomite land in South Africa. *Environ Geol.* 36(1-2):170–178.
- Caramanna G, Ciotoli G, Nisio S. 2008. A review of natural sinkhole phenomena in Italian plain areas. *Nat Hazards.* 45(2):145–172.
- Catani F, Casagli N, Ermini L, Righini G, Menduni G. 2005. Landslide hazard and risk mapping at catchment scale in the Arno River basin. *Landslides.* 2(4):329–342.
- Centamore E, Nisio S, Rossi D. 2009. The San Vittorino Sinkhole Plain: relationships between bedrock structure, sinking processes, seismic events and hydrothermal springs. *Boll Soc Geol Ital.* 128(3): 629–639.
- Ciotoli G, Di Loreto E, Finoia MG, Liperi L, Meloni F, Nisio S, Sericola A. 2016. Sinkhole susceptibility, Lazio region, central Italy. *J Maps.* 12(2):287–294.
- Çoban HO, Öürücü ÖK, Arslan ES. 2020. MaxEnt modeling for predicting the current and future potential geographical distribution of *Quercus libani* Olivier. *Sustainability.* 12(7):2671.
- Convertino M, Troccoli A, Catani F. 2013. Detecting fingerprints of landslide drivers: a MaxEnt model. *J Geophys Res Earth Surf.* 118(3):1367–1386.
- Crosetto M, Monserrat O, Cuevas-González M, Devanthery N, Crippa B. 2016. Persistent scatterer interferometry: a review. *ISPRS J Photogramm Remote Sens.* 115:78–89.
- Dai FC, Lee CF, Ngai YY. 2002. Landslide risk assessment and management: an overview. *Eng Geol.* 64(1):65–87.
- De Filippis L, Anzalone E, Billi A, Faccenna C, Poncia PP, Sella P. 2013. The origin and growth of a recently-active fissure ridge travertine over a seismic fault, Tivoli, Italy. *Geomorphology.* 195:13–26.
- De Ritis R, Nardi A, Materni V, Venuti A, Stefanelli P, Rotella G, Sapia V, Carpentieri E, Tolomei C, Civico R, et al. 2020. Multidisciplinary study of subsidence and sinkhole occurrences in the Acque Albule Basin (Roma, Italy). *Earth Space Sci.* 7(7):1–26. doi:10.1029/2019EA000870
- Del Prete S, Iovine G, Parise M, Santo A. 2010. Origin and distribution of different types of sinkholes in the plain areas of Southern Italy. *Geodin Acta.* 23(1-3):113–127.
- Di Napoli M, Carotenuto F, Cevasco A, Confuorto P, Di Martire D, Firpo M, Pepe G, Raso E, Calcaterra D. 2020. Machine learning ensemble modelling as a tool to improve landslide susceptibility mapping reliability. *Landslides.* 17(8):1897–1914.
- Dursun AE. 2022. Risk analysis of natural sinkholes hazards in Karapınar basin (Konya, Turkey). *Arab J Geosci.* 15(3):1–20.
- Eposito C, Belcicchi N, Bozzano F, Brunetti A, Marmoni GM, Mazzanti P, Romeo S, Cammilozzi F, Cecchini G, Spizzirri M. 2021. Integration of satellite-based A-DInSAR and geological modeling supporting the prevention from anthropogenic sinkholes: a case study in the urban area of Rome. *Geomat Nat Hazards Risk.* 12(1):2835–2864.
- European Environment Agency. 2007. CLC2006 technical guidelines [Internet]. Luxembourg: Publications Office; [accessed 2022 Apr 30]. 10.2800/12134.
- Faccenna C, Soligo M, Billi A, De Filippis L, Funicello R, Rossetti C, Tuccimei P. 2008. Late Pleistocene depositional cycles of the Lapis Tiburtinus travertine (Tivoli, Central Italy): possible influence of climate and fault activity. *Glob Planet Change.* 63(4):299–308.
- Falcioni P. 2018. Rilievi e analisi degli edifici e infrastrutture nelle aree interessate da dissesti e da fenomeni di subsidenza. Report for Guidonia-Montecelio municipality (Rome). <https://www.guidonia.org/>
- Felicísimo ÁM, Cuartero A, Remondo J, Quirós E. 2013. Mapping landslide susceptibility with logistic regression, multiple adaptive regression splines, classification and regression trees, and maximum entropy methods: a comparative study. *Landslides.* 10(2):175–189.
- Floris M, Bozzano F, Strappaveccia C, Baiocchi V, Prestininzi A. 2014. Qualitative and quantitative evaluation of the influence of anthropic pressure on subsidence in a sedimentary basin near Rome. *Environ Earth Sci.* 72(11):4223–4236.
- Forth RA, Butcher D, Senior R. 1999. Hazard mapping of karst along the coast of the Algarve, Portugal. *Eng Geol.* 52(1-2):67–74.
- Galve JP, Gutiérrez F, Remondo J, Bonachea J, Lucha P, Cendrero A. 2009. Evaluating and comparing methods of sinkhole susceptibility mapping in the Ebro Valley evaporite karst (NE Spain). *Geomorphology.* 111(3-4):160–172.
- Galve JP, Remondo J, Gutiérrez F. 2011. Improving sinkhole hazard models incorporating magnitude–frequency relationships and nearest neighbor analysis. *Geomorphology.* 134(1-2):157–170.

- Gao Y, Alexander EC. 2008. Sinkhole hazard assessment in Minnesota using a decision tree model. *Environ Geol.* 54(5):945–956.
- Gasparini C, Di Maro R, Pagliuca NM, Pirro M, Marchetti A. 2002. Recent seismicity of the «Acque Albule» travertine basin. *Ann Geophys.* 45:537–550.
- Giampaolo V, Capozzoli L, Grimaldi S, Rizzo E. 2016. Sinkhole risk assessment by ERT: the case study of Sirino Lake (Basilicata, Italy). *Geomorphology.* 253:1–9.
- Glade T, Crozier MJ. 2005. Hazard impact. *Landslide Hazard Risk.* 43.
- Gomes, VH, Ijff SD, Raes N, Amaral IL, Salomão RP, de Souza Coelho L, de Almeida Matos FD, Castilho CV, de Andrade Lima Filho D, Ramos JF, et al. 2018. Species distribution modelling: contrasting presence-only models with plot abundance data. *Scientific Rep.* 8(1):1–12.
- Guarino PM, Santo A, Forte G, De Falco M, Niceforo DMA. 2017. Analysis of a database for anthropogenic sinkhole triggering and zonation in the Naples hinterland (Southern Italy). *Nat Hazards.* 91(1): 173–192.
- Gutiérrez F, Parise M, De Waele J, Jourde H. 2014. A review on natural and human-induced geohazards and impacts in karst. *Earth-Sci Rev.* 138:61–88.
- Guzzetti F, Reichenbach P, Ardizzone F, Cardinali M, Galli M. 2006. Estimating the quality of landslide susceptibility models. *Geomorphology.* 81(1-2):166–184.
- Intrieri E, Fontanelli K, Bardi F, Marini F, Carlà T, Pazzi V, Di Filippo M, Fanti R. 2018. Definition of sinkhole triggers and susceptibility based on hydrogeomorphological analyses. *Environ Earth Sci.* 77(1): 1–18.
- Intrieri E, Gigli G, Nocentini M, Lombardi L, Mugnai F, Fidinò F, Casagli N. 2015. Sinkhole monitoring and early warning: an experimental and successful GB-InSAR application. *Geomorphology.* 241: 304–314.
- ISPRA. 2022. Sinkhole National Database. Sink Ital Database [Internet]; [accessed 2022 Apr 30]. <http://sgi.isprambiente.it/sinkholeweb/database.html>.
- Javidan N, Kaviani A, Pourghasemi HR, Conoscenti C, Jafarian Z, Rodrigo-Comino J. 2021. Evaluation of multi-hazard map produced using MaxEnt machine learning technique. *Sci Rep.* 11(1):1–20.
- Jaynes ET. 1957. Information theory and statistical mechanics. *Phys Rev.* 106(4):620–630.
- Jenks GF. 1989. Geographic logic in line generalization. *Cartographica.* 26(1):27–42.
- Jiang X, Lei M, Li Y, Dai J. 2005. National-scale risk assessment of sinkhole hazard in China. In: Conference on Sinkholes and the engineering and environmental impacts of Karst, FB Beck eds, ASCE Library, San Antonio, Texas, United States; p. 649–658.
- Kaky E, Nolan V, Alatawi A, Gilbert F. 2020. A comparison between Ensemble and MaxEnt species distribution modelling approaches for conservation: a case study with Egyptian medicinal plants. *Ecol Inform.* 60:101150.
- Kaufmann O, Quinif Y. 2002. Geohazard map of cover-collapse sinkholes in the ‘Tournaisis’ area, southern Belgium. *Eng Geol.* 65(2-3):117–124.
- Kaufmann G, Romanov D. 2019. The initial phase of cave formation: aquifer-scale three dimensional models with strong exchange flow. *J Hydrol.* 572:528–542.
- Kemmerly PR. 1993. Sinkhole hazards and risk assessment in a planning context. *J Am Plann Assoc.* 59(2):221–229.
- Kim YJ, Nam BH, Zheng QP. 2020. An artificial neural network approach to sinkhole hazard assessment for East Central Florida. In: Land L, Kromhout C, Byle M, editors, Proceedings of the 16th Sinkhole Conference: NCKRI Symposium 8, Carlsbad (NM).
- Kleinhans I, Van Rooy JL. 2016. Guidelines for sinkhole and subsidence rehabilitation based on generic geological models of a dolomite environment on the East Rand, South Africa. *J Afr Earth Sci.* 117: 86–101.
- Kornejady A, Ownegh M, Bahremand A. 2017. Landslide susceptibility assessment using maximum entropy model with two different data sampling methods. *Catena.* 152:144–162.
- Koutepov VM, Mironov OK, Tolmachev VV. 2008. Assessment of suffosion-related hazards in karst areas using GIS technology. *Environ Geol.* 54(5):957–962.
- La Rosa A, Pagli C, Molli G, Casu F, De Luca C, Pieroni A, D’Amato Avanzi G. 2018. Growth of a sinkhole in a seismic zone of the northern Apennines (Italy). *Nat Hazards Earth Syst Sci.* 18(9):2355–2366.
- La Vigna F. Modello numerico del flusso dell’unità idrogeologica termominerale delle Acque Albule (Roma). Groundwater numerical flow model of the Acque Albule thermo-mineral hydrogeological unit. Roma T RE University PhD Thesis, <http://hdl.handle.net/2307/434>
- Mora O, Mallorqui JJ, Broquetas A. 2003. Linear and nonlinear terrain deformation maps from a reduced set of interferometric sar images. *IEEE Trans Geosci Remote Sens.* 41(10):2243–2253.

- Nisio S, Caramanna G, Ciotoli G. 2007. Sinkholes in Italy: first results on the inventory and analysis. *SP*. 279(1):23–45.
- Nof RN, Baer G, Ziv A, Raz E, Atzori S, Salvi S. 2013. Sinkhole precursors along the Dead Sea, Israel, revealed by SAR interferometry. *Geology*. 41(9):1019–1022.
- Notti D, Herrera G, Bianchini S, Meisina C, García-Davalillo JC, Zucca F. 2014. A methodology for improving landslide PSI data analysis. *Int J Remote Sens*. 35(6):2186–2214.
- Orhan O, Yakar M, Ekerin S. 2020. An application on sinkhole susceptibility mapping by integrating remote sensing and geographic information systems. *Arab J Geosci*. 13(17):1–17.
- Ozdemir A. 2016. Sinkhole susceptibility mapping using logistic regression in Karapınar (Konya, Turkey). *Bull Eng Geol Environ*. 75(2):681–707.
- Papathoma-Köhle M, Neuhäuser B, Ratzinger K, Wenzel H, Dominey-Howes D. 2007. Elements at risk as a framework for assessing the vulnerability of communities to landslides. *Nat Hazards Earth Syst Sci*. 7(6):765–779.
- Parise M, Vennari C. 2013. A chronological catalogue of sinkholes in Italy: the first step toward a real evaluation of the sinkhole hazard. Proceedings of the 13th Sinkhole Conference, May 2013, Carlsbad, New Mexico.
- Pazzi V, Di Filippo M, Di Nezza M, Carlà T, Bardi F, Marini F, Fontanelli K, Intrieri E, Fanti R. 2018. Integrated geophysical survey in a sinkhole-prone area: microgravity, electrical resistivity tomographies, and seismic noise measurements to delimit its extension. *Eng Geol*. 243:282–293.
- Pellicani R, Van Westen CJ, Spilotro G. 2014. Assessing landslide exposure in areas with limited landslide information. *Landslides*. 11(3):463–480.
- Perino G, Sileno L, Tresalli GO. 2018. Costi teorici di costruzione e di manutenzione. *Contrib Ric*. 263: 70–71.
- Phillips SJ, Anderson RP, Schapire RE. 2006. Maximum entropy modeling of species geographic distributions. *Ecol Model*. 190(3–4):231–259.
- Phillips SJ, Dudík M, Schapire RE. 2021. Maxent software for modeling species niches and distributions (Version 3.4.1). [accessed 2018 May 21]. https://biodiversityinformatics.amnh.org/open_source/maxent/.
- Raso E, Di Martire D, Cevasco A, Calcaterra D, Scarpellini P, Firpo M. 2020. Evaluation of prediction capability of the MaxEnt and Frequency Ratio methods for landslide susceptibility in the Vernazza catchment (Cinque Terre, Italy). In: *Applied geology*. Cham (Switzerland): Springer; p. 299–316.
- Rinalduzzi S, Farroni L, Billi A, De Filippis L, Faccenna C, Poncia PP, Spadafora G. 2017. Geocultural landscaping: guidelines and conceptual framework to design future scenarios of exploited lands. *Land Use Policy*. 64:258–281.
- Rispoli C, Di Martire D, Calcaterra D, Cappelletti P, Graziano SF, Guerriero L. 2020. Sinkholes threatening places of worship in the historic center of Naples. *J Cult Herit*. 46:313–319.
- Santo A, Ascione A, Del Prete S, Di Crescenzo G, Santangelo N. 2012. Collapse sinkholes in the carbonate massifs of Central and Southern Apennines. *AC*. 40(1):95–112.
- Shannon CE. 1948. A mathematical theory of communication. *Bell Syst Tech J*. 27(3):379–423.
- Sinharay S. 2010. Jackknife methods. In: Peterson P, Baker E, McGaw B editors, *International encyclopedia of education*: Elsevier Ltd; p. 229–231. <https://doi.org/10.1016/B978-0-08-044894-7.01338-5>.
- Solari L, Barra A, Herrera G, Bianchini S, Monserrat O, Béjar-Pizarro M, Crosetto M, Sarro R, Moretti S. 2018. Fast detection of ground motions on vulnerable elements using Sentinel-1 InSAR data. *Geomat Nat Hazards Risk*. 9(1):152–174.
- Taheri K, Gutiérrez F, Mohseni H, Raeisi E, Taheri M. 2015. Sinkhole susceptibility mapping using the analytical hierarchy process (AHP) and magnitude–frequency relationships: a case study in Hamadan province, Iran. *Geomorphology*. 234:64–79.
- Theron A, Engelbrecht J, Kemp J, Kleynhans W, Turnbull T. 2017. Detection of sinkhole precursors through SAR interferometry: radar and geological considerations. *IEEE Geosci Remote Sensing Lett*. 14(6):871–875.
- Toulkeridis T, Rodríguez F, Arias Jiménez N, Baile DS, Martínez RS, Addison A, Carreón Freyre D, Mato F, Díaz Perez C. 2016. Causes and consequences of the sinkhole at El Trébol of Quito, Ecuador—implications for economic damage and risk assessment. *Nat Hazards Earth Syst Sci*. 16(9): 2031–2041.
- Townsend Peterson A, Papeş M, Eaton M. 2007. Transferability and model evaluation in ecological niche modeling: a comparison of GARP and Maxent. *Ecography*. 30(4):550–560.
- Tufano R, Guerriero L, Annibali Corona M, Bausilio G, Di Martire D, Nisio S, Calcaterra D. 2022. Anthropogenic sinkholes of the city of Naples, Italy: an update. *Nat Hazards*. 112(3):2577–2608. [accessed 2022 May 11].

- Waltham T, Bell FG, Culshaw MG, Knez M, Slabe T. 2005. Sinkholes and subsidence: karst and cavernous rocks in engineering and construction. Vol. 382. Berlin, Germany: Springer.
- Watson RA, Holohan EP, Al-Halbouni D, Saberi L, Sawarieh A, Closson D, Alrshdan H, Abou Karaki N, Siebert C, Walter TR, et al. 2019. Sinkholes and uvalas in evaporite karst: spatio-temporal development with links to base-level fall on the eastern shore of the Dead Sea. *Solid Earth*. 10(4):1451–1468.
- Yilmaz I. 2007. GIS based susceptibility mapping of karst depression in gypsum: a case study from Sivas basin (Turkey). *Eng Geol*. 90(1-2):89–103.